MIDA-Boronate Monomers in Suzuki-Miyaura

Catalyst-Transfer Polymerization: the Pros and Cons

Mitchell T. Howell, *Frank R. Fronczek, *and Evgueni E. Nesterov**, *

[†]Department of Chemistry and Biochemistry, Northern Illinois University, DeKalb, Illinois 60115, USA. E-mail: een@niu.edu

[‡]Department of Chemistry, Louisiana State University, Baton Rouge, Louisiana 70803, USA

For Table of Contents use only

ABSTRACT. Controlled polymerization for the synthesis of structurally precise conjugated polymers remains a challenging problem in polymer chemistry. Catalyst-transfer polymerization (CTP) based on Pd-catalyzed Suzuki-Miyaura cross-coupling is one of the promising approaches toward solving this challenge. Recent introduction of *N*-methyliminodiacetic acid (MIDA) boronates as monomers for Suzuki-Miyaura CTP has extended this approach towards a broader variety of monomer structures and led to improved control over the polymerization, particularly for heteroaromatic systems (such as thiophenes). Previously, we found that MIDA-boronate monomers polymerization could be facilitated

by Ag⁺-mediated reaction conditions due to shifting the Pd catalytic cycle toward a more efficient oxo-Pd transmetalation pathway where MIDA-boronates could participate in transmetalation directly, without prior hydrolysis to boronic acid. In this work, we continued studying this novel process, and investigated the dual role of the MIDA-boronate functional group in the case of less reactive fluorenyl (and potentially other all-carbon aromatic systems) monomers. With such monomers, MIDA-boronate group enables the controlled polymerization but also produces a hydrolysis byproduct hindering the polymerization. We also investigated the role of Ag⁺ acting to counteract this hindering effect. Steric bulkiness of the MIDA-boronate functional group may also slow down the Suzuki-Miyaura CTP process. These complications could reduce the synthetic value of MIDA-boronate monomers in Suzuki-Miyaura CTP, although better understanding of these implications and a proper choice of polymerization conditions and catalytic initiators could to some extent mitigate such problems. As part of this work, we also uncovered a "critical length" phenomenon which results in a dual molecular weight distribution of the resulting conjugated polymer, both with MIDA-boronate and boronic acid monomers. This phenomenon could account for the experimentally observed loss of polymerization control beyond formation of the polymer chains of a certain "critical length", even despite the formally "living" nature of the polymer chains. The generality of this phenomenon and whether it is restricted to using Pd catalytic systems based on Buchwald-type phosphine ligands remains to be studied. Overall, these new findings paint a sophisticated picture of the Suzuki-Miyaura CTP process with MIDA-boronate monomers where the mere presence of a Pd center on the polymer chain is not sufficient to sustain the polymerization (even if a chain could be considered "living" in a sense of possessing a Pd center), and the choice of phosphine ligand on the Pd center is an effective tool to overcome the "critical length" restriction.

Introduction

Since the historic discovery of conductivity in extended π -conjugated polymers, the precise, controllable, and reproducible synthesis of complex and novel π -conjugated organic polymers has become a major milestone goal towards the advancement of organic electronic materials. New efficient methods that reliably yield π -conjugated organic polymers are often hinged on adapting conventional small-molecule bond forming cross-coupling reactions for living/controlled chain-growth polymerization processes. Not only has this reaction adaptation approach been successfully used in polymer synthesis but it also has provided valuable information on the reaction mechanisms themselves. For example, two recently published perspectives by McNeil and Luscombe discussed how the studies of Suzuki-Miyaura catalyst-transfer polymerization and direct arylation polymerization enabled better understanding of the underlying small-molecule cross-coupling processes and led toward enhanced reaction designs. Not only has this reaction designs.

After the first practical demonstration by Yokozawa for the synthesis of polyfluorenes,⁸ the controlled Suzuki-Miyaura catalyst-transfer polymerization (SCTP) has experienced much advancement as a versatile method for the preparation of various π -conjugated organic polymers (CPs).⁹

In SCTP, monomer units are attached to the reactive end of the growing polymer chain via the formation of a new carbon-carbon bond through Suzuki-Miyaura cross-coupling while the controlled (or living) nature of the polymerization stems from catalyst migration across the π -system via a series of Pd⁰ π -complexes until oxidative addition occurs at a terminal carbon-halide bond (Figure 1a). When using high-reactivity thiophene based monomers, initial issues of low yielding polymerizations paired with poor control of polymer molecular weight and coupling defects caused by competitive reaction pathways were addressed by Turner *et al.* via the use of *N*-methyliminodiacetic acid (MIDA) protected boronates (Ar-BMIDA) as monomers for the synthesis of polythiophenes.¹⁴ At that time, it was hypothesized that the MIDA-boronate group would slowly hydrolyze in the mildly basic conditions of polymerization creating a steady small concentration of a reactive boronic acid monomer (Ar-B(OH)₂),

and hence would improve the polymerization outcome through the reduced probability of the side reactions (e.g. protodeboronation). This approach was later implemented and further modified by Choi et. al. through the use of Buchwald Pd pre-catalyst initiators to result in a more uniform initiation stage leading to narrow dispersity and controlled molecular weight in the preparation of polythiophenes. 15, 16 Following that work, Choi and others later expanded the scope of this method to a wider variety of heterocyclic monomers through structural modifications of the Ar-BMIDA unit to fine-tune the reactivity of the monomer. 17-21 Recently, we investigated the possibility to expand using MIDAboronate monomers in SCTP toward all-carbon aromatic monomers (such as fluorenes).²² While fluorenyl MIDA-boronate monomers were inefficient in SCTP in the original set of reaction conditions, we found that the presence of Ag⁺ in reaction medium during polymerization helped to steer the Suzuki cross-coupling step towards the more efficient oxo-Pd transmetalation pathway and away from the less efficient boronate transmetalation pathway (Figure 1b). At the same time, through a kinetic study of the polymerization process, we demonstrated that the Ar-BMIDA monomer was able to participate in a **direct** transmetalation step under these Ag⁺-mediated conditions rather than to simply produce a steady low concentration of the corresponding boronic acid monomer via a slow hydrolysis of the MIDAboronate group.

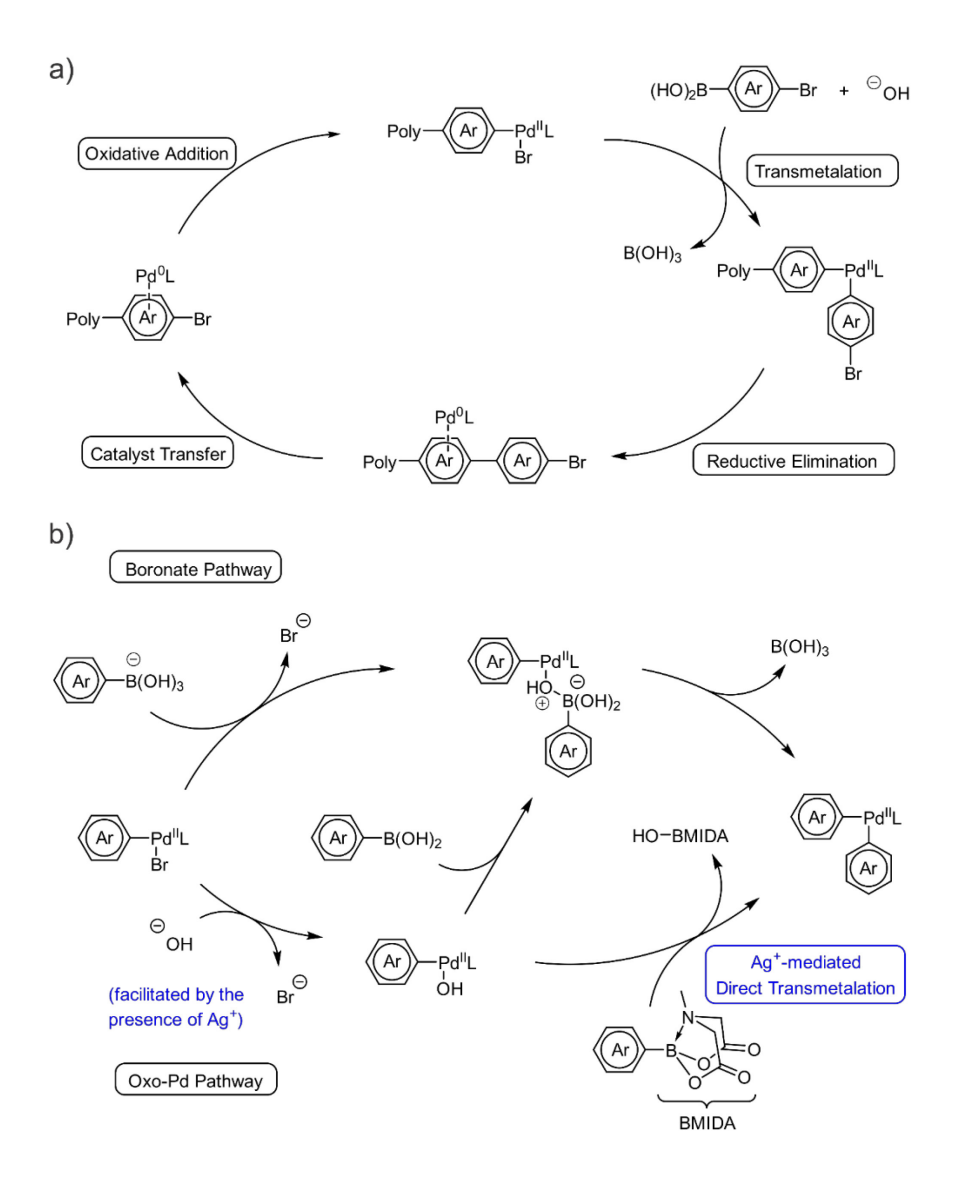


Figure 1. (a) The accepted mechanism of Suzuki-Miyaura catalyst-transfer polymerization (SCTP). (b) Two alternative pathways (boronate and oxo-Pd) for the transmetalation step in Suzuki-Miyaura cross-coupling mechanism. The direct transmetalation route (in oxo-Pd pathway) available to MIDA-boronates in Ag⁺-mediated conditions is also shown.

Our previous study concerning the finding of the direct Ar-BMIDA transmetalation in Suzuki-Miyaura cross-coupling left some key mechanistic questions on the role of MIDA-boronates in SCTP unanswered and hence they became the focus of this work. One observation of note was that the presence of a Ag⁺ source was a crucial requirement to facilitate polymerization of the Ar-BMIDA monomer even though simultaneous hydrolysis of the BMIDA group to form Ar-B(OH)₂ monomer was occurring in the reaction conditions. Surprisingly, the thus formed Ar-B(OH)₂ monomer was found to

be nearly unreactive in the Ag⁺-mediated polymerization conditions, and hence it accumulated in the reaction mixture. This observation was baffling given that, in a separate run, when Ar-B(OH)₂ was used as a monomer, we did observe efficient formation of the target polymer through SCTP. It also raised a more general question on the role of the MIDA-boronate group in SCTP process. These issues are addressed in this study where we demonstrate that the MIDA-boronate group hydrolysis by-product, MIDA itself, can inhibit SCTP of an Ar-B(OH)₂ monomer. We also found that added Ag⁺ can counteract the inhibitory effect of MIDA and thus allow the polymerization to proceed. In addition, in this study we aimed at better understanding the direct Ar-BMIDA transmetalation process itself. In so doing, the nature of the Pd catalytic initiator and how it relates to the direct Ar-BMIDA transmetalation was further investigated. Lastly, based on study of the polymer chain composition, we introduced a novel concept of "critical length" that enabled better mechanistic description of the SCTP with less reactive monomers.

Results and Discussion

The detrimental role of MIDA on SCTP and mitigating effect of Ag^+ . Poly(9,9-dioctylfluorene) (PF), which is a popular blue-emitting polymer material for designing organic LEDs, ²³⁻²⁶ was chosen as a model polymer system for the study. This polymer was the target of our previous work, ²² so it was a natural choice for continuing the investigation. The fluorenyl monomers, like 1 and 2 (Figure 2a), are generally less efficient in SCTP (compared to analogous heterocyclic monomers, i.e. thiophenes) due to the weaker Pd^0 binding in the π -complex (which is required to sustain a catalyst-transfer process) as well as the requirement for an active Pd^0 center to ring-walk over two adjacent phenylene units in the catalyst-transfer step. ¹¹ The overall lower efficiency of the fluorenyl monomers in SCTP was considered desirable in mechanistic studies as the process would be more sensitive to reaction conditions and the catalyst's structure.

Figure 2. (a) Reaction conditions for the preparation of polyfluorene (PF) using SCTP. (b) Synthesis and structures of catalytic initiators **4-8** used in this study.

Two fluorenyl monomers were used in this study: monomer 1 was functionalized with a MIDA-boronate group and monomer 2 bore an unprotected boronic acid group. The polymerization reaction conditions are outlined in Figure 2a and Table 1. External catalytic initiators 4-8 were prepared starting from a readily available COD-palladacycle 3 through a modular synthesis recently described by Buchwald²⁷ (Figure 2b) which provided full control over both the ligand and aryl functionality of the initiating catalyst without formation of undesired by-products. Using the pre-synthesized pure and structurally homogeneous catalytic initiators (as opposed to *in situ* generated catalytic initiators described in previous works) allowed for more accurate control over the monomer to catalytic initiator feed ratio (M_0/I_0). As a Ag^+ source, we used Ag_2SO_4 due to its low solubility in the reaction media and hence the ability to deliver steady low solution concentration of Ag^+ , therefore preventing undesired consumption of Ag^+ into insoluble Ag_2O under the basic reaction conditions. Polymerizations with Ar-

BMIDA monomer 1 were done within reaction times that did not allow complete polymerizations in order to explore comparative reaction efficiencies in various reaction conditions.

Table 1. Ag⁺-mediated SCTP of monomers 1 and 2. ^a

Entry	Monomer	Catalytic initiator	Ag ₂ SO ₄	M_0/I_0	Yield ^b (%)	M _n ^c (kDa)	M _w ^c (kDa)	D^{c}
1	1	4	_	24:1	1	4.14	6.01	1.45
2	1	4	+	24:1	41	4.95	5.76	1.16
3	2	4	_	24:1	70	7.20	10.30	1.43
4 ^d	2	4	_	24:1	50	7.52	9.34	1.29
5 ^e	2	4	_	24:1	33	4.58	5.60	1.22
6	2	4	+	24:1	74	12.05	16.11	1.34
7 ^d	2	4	+	24:1	70	11.21	17.85	1.60
8 ^e	2	4	+	24:1	76	12.69	24.14	1.98
9	1	5	+	24:1	41	8.53	10.91	1.28
10	1	6	+	24:1	47	5.00	7.02	1.40
11	1	7	+	24:1	30	4.40	4.99	1.13
12	1	8	+	24:1	30	4.63	6.50	1.41
13 ^f	1	4	+	12:1	42	5.66	7.76	1.07
14 ^f	1	4	+	24:1	54	8.76	14.69	1.67
15 ^f	1	4	+	36:1	41	9.23	17.34	1.88
16 ^f	1	4	+	48:1	27	8.15	17.06	1.97
17	2	4	_	12:1	76	4.08	5.30	1.30
18	2	4	_	36:1	67	9.88	15.25	1.54
19	2	4	_	48:1	67	11.00	18.83	1.71

^a Reaction conditions: 10 eq. K₃PO₄, 0.5 eq. Ag₂SO₄ (unless indicated otherwise), temperature 30 °C, solvent THF with 5% v/v water, reaction time 24 h; ^b Isolated polymer yield by weight; ^c Determined with GPC using THF as eluent and calibrated against polystyrene standards; ^d Polymerization was carried out in the presence of 1 eq. of added MIDA; ^e Polymerization was carried out in the presence of 3 eq. of added MIDA; ^f Reaction time 40 h.

The puzzling observation that MIDA-boronate monomer 1 can only polymerize in the presence of equimolar amount of Ag⁺ (i.e. 0.5 eq. of Ag₂SO₄) is illustrated by entries 1 and 2 in Table 1. Two runs with M_0/I_0 feed ratio of 24 (theoretical M_n 9.5 kDa) were done over 24 h reaction time in the absence and presence of 0.5 eq. of Ag₂SO₄. Although neither polymerization reached completion in the allocated reaction time, the polymerization essentially did not occur without Ag+ source as indicated by a negligible PF isolated yield of 1%. In contrast, in the presence of Ag₂SO₄ a moderate yield of 41% of the polymer with number average molecular weight M_n 4.95 kDa and narrow dispersity (D 1.16) was obtained. Similar polymerizations were carried out with boronic acid monomer 2. In this case, polymerization readily occurred without added Ag₂SO₄ producing PF with a near expected molecular weight (M_n 7.20 kDa, D 1.43) and good yield of 70% (entry 3 in Table 1). The addition of Ag₂SO₄ under the same conditions (entry 6 in Table 1) resulted in a similar yield of the polymer (74%) but with a higher $M_{\rm n}$ 12.05 kDa (D 1.34). Therefore, the boronic acid monomer 2 could polymerize in the conditions with or without Ag₂SO₄ and in both cases more efficiently than the Ar-BMIDA monomer 1 under the same reaction conditions. This striking comparison led to an intriguing question of why there was little-to-no polymerization observed when Ar-BMIDA monomer 1 was used in the absence of Ag₂SO₄ even though slow hydrolysis of the MIDA-boronate to boronic acid group simultaneously occurred in the reaction conditions to generate the boronic acid monomer 2?

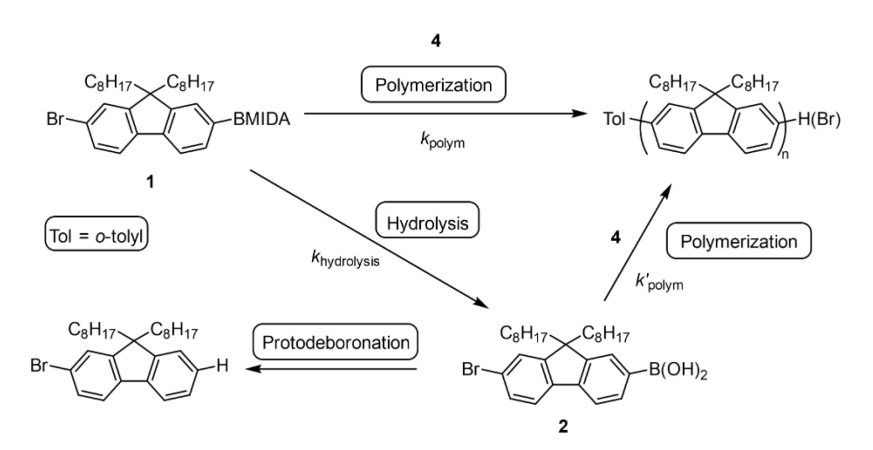


Figure 3. Processes occurring during polymerization of MIDA-boronate monomer 1.

To investigate this puzzling observation, we carried out a series of kinetic studies to better understand the polymerization mechanism with both monomers. First, we re-examined the possibility of direct MIDA-boronate transmetalation to occur in the Ag⁺-mediated conditions, given the change of base to K₃PO₄ in this study (the previous study utilized Cs₂CO₃ as a base²²). To obtain polymerization kinetic data, small aliquots were withdrawn at various times during polymerization, and the polymer product was analyzed by GPC (Figure 3, more experimental details are in the Supporting Information). The polymerization of MIDA-boronate monomer 1 in the presence of Ag⁺ displayed a pseudo first-order kinetics, and from the linear dependence of $ln(M_n)$ over time a rate constant k_{polym} 0.085 h^{-1} was obtained (Figure S1 in the Supporting Information). Polymerization kinetics were not examined for the polymerization of 1 in conditions without Ag⁺ given the inability to substantially produce polymer product. We also studied the hydrolysis kinetics of monomer 1 under the employed polymerization conditions (aqueous THF, milder base). MIDA-boronate was expected to undergo slow hydrolysis to form boronic acid monomer 2 (Figure 3).²⁸ The small aliquots were withdrawn during the reaction and analyzed using ¹H NMR spectroscopy. In the presence of Ag⁺, we obtained the first-order rate constant $k_{\text{hydrolysis}} 0.029 \text{ h}^{-1}$ (Figure S2 in the Supporting Information). A similar value of the hydrolysis rate constant ($k_{hydrolysis}$ 0.033 h⁻¹) was obtained in the conditions without added Ag⁺ thus indicating that the presence of Ag⁺ did not influence hydrolysis of the MIDA-boronate group under the reaction conditions. Since $k_{\text{polym}} > k_{\text{hydrolysis}}$, one had to conclude that MIDA-boronate 1 was participating in the polymerization directly, without preceding hydrolysis to boronic acid monomer 2, and therefore the direct transmetalation pathway involving the MIDA-boronate group was operative under the given reaction conditions using K₃PO₄ as a base. This followed our previous observations when using Cs₂CO₃ as a base.²² When performing kinetic studies, we also noticed that there was a substantial delay in SCTP initiation resulting in PF polymer formation with substantially high molecular weight only after 10 h of reaction time. This initiation delay will be addressed later in the paper.

In a similar vein, the polymerization kinetics was studied with the boronic acid monomer $\mathbf{2}$, both in the conditions with and without the presence of Ag₂SO₄ (Figure S3 in the Supporting Information). Without Ag₂SO₄ in the reaction medium, we found the pseudo first-order polymerization rate constant k'_{polym} 0.73 h⁻¹, whereas in the conditions with Ag₂SO₄ the rate constant k'_{polym} 2.07 h⁻¹ was obtained. Both rate constants for the polymerization of boronic acid monomer $\mathbf{2}$ were found to be significantly higher than the corresponding rate constants for polymerization of MIDA-boronate monomer $\mathbf{1}$. This reflected high reactivity of the boronic acid monomer $\mathbf{2}$ to participate in SCTP thus further exacerbating the shocking inability of the monomer $\mathbf{1}$ to polymerize in the absence of Ag₂SO₄. We also noticed the beneficial effect of Ag⁺ presence on the polymerization rate of the monomer $\mathbf{2}$, likely stemming from Ag⁺ enforcing the more efficient oxo-Pd transmetalation pathway (as was observed in our previous work²²).

To explain the inefficient polymerization of Ar-BMIDA monomer 1 in the absence of Ag_2SO_4 , we initially hypothesized that a protodeboronation process might be competing with polymerization for the consumption of the slowly formed Ar-B(OH)₂ monomer 2 (Figure 3).^{29, 30} To better evaluate this possibility, the composition of the reaction mixture was analyzed for the polymerization of 1 in the absence of Ag_2SO_4 (the reaction was carried out in the conditions of entry 1 in Table 1 for the total reaction time 10 h). The mole fraction composition of the small-molecule fluorenyl components was determined through ¹H NMR analysis of the concentrated mother liquor obtained after polymer precipitation in acetone. The analysis indicated that 72% of the Ar-BMIDA monomer 1 remained intact while 24% hydrolyzed and accumulated as the Ar-B(OH)₂ monomer 2. The obtained amount of boronic acid 2 matched the amount that could be calculated based on the experimental value of pseudo first-order kinetic rate constant $k_{hydrolysis}$. The remaining 4% of monomer 1 converted to PF polymer (M_n 3.21 kDa, D 1.13). Importantly, no protodeboronation product was observed in the ¹H NMR spectra of the isolated mother liquor. Therefore, given the accumulation of Ar-B(OH)₂ monomer 2 and absence of the protodeboronation product, we could conclude that protodeboronation was not a substantial

factor, and some other factors must be preventing the polymerization of Ar-B(OH)₂ monomer **2** from occurring.

Until this point, N-methyliminodiacetic acid (MIDA) (or its dicarboxylate) that is formed as a product of hydrolysis of MIDA-boronate monomer 1 in the SCTP reaction conditions had been considered an inert spectator. Yet, the presence of this compound in an equimolar amount with boronic acid 2 is a distinct difference between the polymerization of 2 formed through an in situ hydrolysis of MIDA-boronate 1 and the polymerization of neatly taken 2, thus making MIDA the possible suspect for inhibiting polymerization of 2. To evaluate this conjecture, we carried out polymerizations of Ar-B(OH)₂ monomer 2 in the absence of added Ag⁺ in the identical reaction conditions but with added 1 eq. or 3 eq. of MIDA (compare entry 3 with entries 4 and 5 in Table 1). A clear detrimental impact of added MIDA on the polymerization was observed as both M_n and yield of the polymer were suppressed with the increasing amount of MIDA. We also observed that the addition of Ag₂SO₄ could mitigate the negative impact of MIDA on the polymerization (compare entry 6 with entries 7 and 8 in Table 1) as both the yield and M_n of the obtained polymers were not substantially affected by the MIDA presence. Therefore, we concluded that the inefficient SCTP of MIDA-boronate monomer 1 in the conditions without Ag₂SO₄ could be explained by a hindering effect imparted by the accumulation of free MIDA through a slow hydrolysis of MIDA-boronate 1.

Mechanistic aspects of the MIDA interaction with Pd species participating in SCTP. We first checked if the hindering effect of MIDA on polymerization of boronic acid monomer 2 could be due to MIDA forming a stable complex with the catalytic aryl-Pd^{II} species involved in the reaction mechanism. MIDA's ability to chelate with Pd^{II} has been documented in the literature.^{31, 32} The Pd-RuPhos catalytic initiator 4 was stirred with 30 eq. of K₃PO₄ and 30 eq. of MIDA in 10% v/v D₂O-THF for 16 h at 30 °C to mimic polymerization conditions. ³¹P NMR spectrum of the reaction mixture showed an unchanged resonance signal at 25.1 ppm when compared to the neat catalytic initiator 4 and no other signals in ³¹P NMR spectrum could be detected. This demonstrated that MIDA produced

through hydrolysis of Ar-BMIDA monomer 1 did not appear to form any detectable complex with aryl-Pd^{II} species under these conditions. In a similar manner, MIDA's ability to interact with Ar-B(OH)₂ was also examined via ¹H NMR spectroscopy and showed no interaction. The overall lack of interaction between both prominent chemical species involved in Suzuki-Miyaura cross-coupling suggested that MIDA could alternatively disrupt the SCTP catalytic cycle through interaction with an active Pd⁰ species formed by the reductive elimination step and responsible for robustness of the chain-growth mechanism.

Figure 4. Effect of MIDA on small-molecule cross-coupling. The mixture composition (relative molar fractions) was determined from relative intensities of the corresponding GC-MS signals after quenching the reaction mixture with 1 M HCl and extracting with CH₂Cl₂.

To test MIDA's ability to interfere with the Pd⁰(RuPhos) species, a small-molecule cross-coupling reaction between 1 eq. of the Pd-RuPhos catalytic initiator 4 and 1 eq. of phenylboronic acid 9 was investigated in both absence and presence of 3 eq. of MIDA (Figure 4). When performing the reaction in the conditions without MIDA, the mixture rapidly developed a wine-red color upon adding the reagents, and turned brown and turbid after stirring at 30 °C for 5 min. After the reaction mixture was quenched with 1 M HCl, it was analyzed using GC-MS. In addition to formation of the expected cross-coupling product 10 (relative molar fraction 65 mol%), we also detected biphenyl 11 (35 mol%) (Figure S5 in the Supporting Information). Formation of biphenyl could be attributed to a competitive homocoupling of phenylboronic acid 9. This side reaction is known to be catalyzed by Pd⁰ species, 33, 34 and hence indicates that free Pd⁰(RuPhos) species was available in the reaction medium following the reductive elimination step. The same reaction was done in the presence of 3 eq. MIDA; the reaction

mixture slowly turned orange over 30 min. A GC-MS analysis of the reaction mixture (after quenching with 1 M HCl) revealed formation of the cross-coupling product 10 (40 mol%), along with orthoiodotoluene 12 (20 mol%) and unreacted boronic acid 9 (40 mol%, as a cyclic trimeric anhydride) (Figure S6 in the Supporting Information). Formation of the cross-coupling product 10 indicated that both transmetalation and reductive elimination steps were not affected by the presence of MIDA. However, the effect of MIDA presence was noticeable and could be attributed to MIDA being able to effectively intercept a Pd⁰(RuPhos) complex in solution. Such a "trapping" of Pd⁰ complex could facilitate reverse reductive elimination in 4 leading to ortho-iodotoluene (Figure 4), and would decrease the amount of 4 available for coupling with 9, leading to substantial amount of unreacted boronic acid 9. The absence of the free Pd⁰(RuPhos) complex in solution was responsible for no biphenyl formation via homocoupling of boronic acid 9, despite its substantial presence in the reaction conditions. Although all these findings indirectly pointed on the essential interaction between Pd⁰(RuPhos) complex and MIDA, our attempts to directly observe such an interaction using ³¹P NMR spectroscopy, or to isolate a complex formed between these two species proved unsuccessful. Therefore, we decided to evaluate the effect of MIDA on the Pd⁰ catalyst-transfer step.

Figure 5. Study of the effect of MIDA on catalyst-transfer efficiency. The product mixture composition (relative amounts of products **10** and **15** and unreacted dibromofluorene **13**) was determined using ¹H NMR spectroscopy after quenching the reaction mixture with 1 M HCl and extracting with CH₂Cl₂.

To evaluate the effect of MIDA on the $Pd^{0}(RuPhos)$ π -complex in the catalyst-transfer step, we performed a cross-coupling reaction between equimolar amounts of phenylboronic acid 9 and dibromofluorene 13 (Figure 5). This is a common test used to study catalyst-transfer ability of various aromatic monomers involved in catalyst-transfer polymerizations. 35, 36 We carried out this reaction in the absence of MIDA, and with 1 and 3 eq. of MIDA present. The mole fraction ratios for the monocoupling product 14 and the di-coupling product 15 were determined through ¹H NMR analysis of the crude reaction mixtures (after quenching with 1 M HCl) with respect to the dibromofluorene 13. A larger fraction of 15, with a maximum of 0.5, would indicate a better Pd⁰(RuPhos) ring-walking (catalyst-transfer) efficiency. The reaction with no MIDA gave the di-coupling product 15 only, with no detectable mono-coupling product 14. Integration of the ¹H NMR signals for 13 and 15 (Figure S7) in the Supporting Information) gave the molar fraction of 15 at 0.34. We also noticed presence of the product 10 (molar fraction 0.07) from the initial coupling of 4 with phenylboronic acid 9 - a step preceding the formation of the Pd⁰(RuPhos) species. These results demonstrated that in the absence of MIDA, Pd⁰(RuPhos) species could be readily formed from the initial coupling event, successfully perform oxidative addition with dibromofluorene 13 and effectively undergo catalyst migration across the fluorenyl π -system to result in the di-coupling product 15.

The addition of MIDA, 1 and 3 eq., to the cross-coupling reaction also produced solely the dicoupling product **15** albeit with diminishing molar fractions of 0.25 and 0.08, respectively (Figure 5). Still, the lack of detectable mono-coupling product **14** implied that MIDA did not interfere with $Pd^0(RuPhos)$ migration across the fluorenyl π -system. A substantial amount of unreacted boronic acid **9** was also observed, as well as unreacted dibromofluorene **13**, especially in the case of 3 eq. of MIDA. The amount of the initial coupling product **10** was unchanged by the presence of MIDA (molar fraction about 0.07 in all the cases). Overall, this experiment indicated that presence of MIDA had no impact on the transmetalation and reductive elimination steps nor it affected the catalyst-walking ability of $Pd^0(RuPhos) \pi$ -complex species. Still, MIDA presence has resulted in the significant decrease of cross-

coupling efficiency toward product **15**. It appears that the MIDA detrimental impact on cross-coupling could be associated with effective intercepting a free Pd⁰(RuPhos) species in solution. However, expanding this conclusion from a small-molecule cross-coupling to the SCTP process is not that straightforward given that once a polymer chain has been initiated, it should remain active provided that the catalyst-transfer across a single fluorenyl unit is unaffected by MIDA presence and hence should allow polymerization to potentially continue even in the presence of MIDA. Of course, a single fluorenyl unit does not completely account for the structure of a growing PF chain in which Pd⁰ π -complexation may be more susceptible to MIDA presence given the increased chain length.³⁷ With some hints from small-molecule cross-coupling pointing on a possible reason, further additional research will help in elucidating the exact mechanism of MIDA acting to disrupt SCTP.

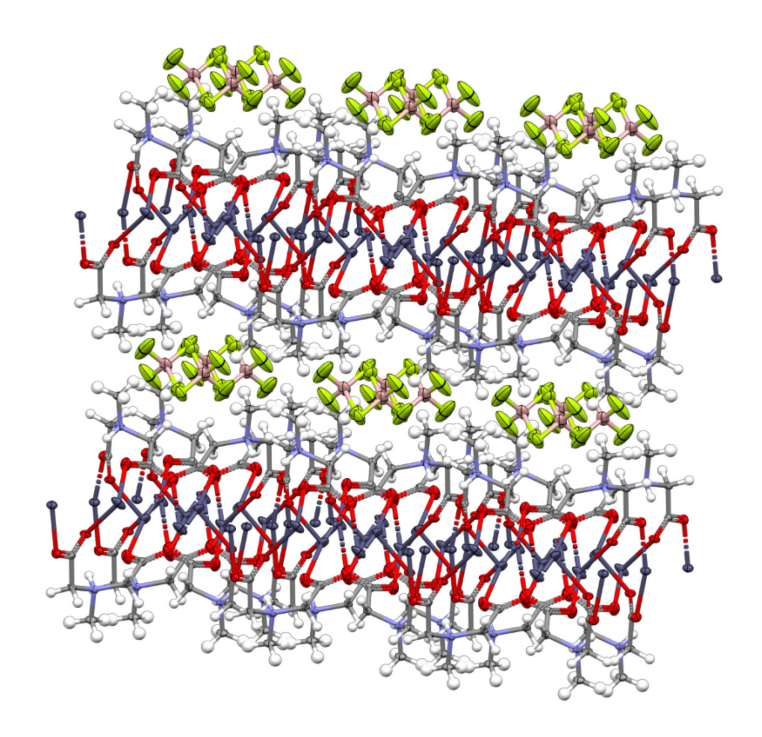


Figure 6. A fragment of a layered structure of the Ag-carboxylate polymer prepared upon AgBF₄ reaction with MIDA. The structure was obtained from X-ray crystallographic data. Ellipsoid drawing is shown at the 50% level for all atoms except hydrogens.

Since MIDA is capable of inhibiting the SCTP process through entrapment of the free Pd⁰ complex in solution, the beneficial effect of added Ag⁺ in mitigating the negative impact of MIDA

accumulation could be through the formation of an insoluble in the reaction conditions Ag-MIDA complex that could effectively remove MIDA from the reaction medium. In order to confirm this, we stirred a mixture of a THF-soluble salt AgBF₄ with MIDA in THF at 30 °C. We observed quantitative formation of a colorless precipitate. Although the precipitate was not soluble in THF, it was soluble in water upon heating, and could be recrystallized from hot water. ¹H NMR spectrum of the product exhibited broad signals from MIDA CH₂ and CH₃ groups indicating that the product was a MIDA complex. Single-crystal X-ray crystallography revealed that this was a Ag-carboxylate supramolecular polymer with a composition [Ag₃(MIDA-H)₂]⁺BF₄⁻, where MIDA-H refers to the MIDA-dicarboxylate ligand protonated at N atom (Figure 6). The polymer had a layered structure with tightly packed Agcarboxylate two-dimensional polymer layers separated by the layers of BF₄⁻ anions. A similar polymeric Ag-carboxylate compound possibly forms in the basic reaction conditions of SCTP process where its low solubility enables an effective removal of the free MIDA compound thus precluding its accumulation in the active form. The role of Ag⁺ as a MIDA "scavenger" is synergistic to the role of Ag⁺ as a facilitator of the more efficient oxo-Pd transmetalation pathway therefore further enhancing the SCTP reactivity of the MIDA-boronate monomer 1.

Aryl moiety in the catalytic initiator and the polymerization rate. Studies of the Ag⁺-mediated polymerization kinetics of the MIDA-boronate monomer 1 with the *ortho*-tolyl catalytic initiator 4 produced a relatively low observed kinetic rate (characterized by a pseudo first-order rate constant k_{polym} 0.085 h⁻¹). Meanwhile, we noticed that there was almost no polymer produced in the first 10 h of polymerization reaction but the polymer production would catch up in the subsequent period between 11 and 24 h polymerization time. From the analysis of composition of the reaction mixture at 11 h polymerization time, we estimated a pseudo first-order polymerization rate constant k_{polym} 0.01 h⁻¹, which was substantially lower than the polymerization rate constant obtained for the longer polymerization runs. Thus, this indicated a significant initiation delay in the earlier stage of the polymerization of MIDA-boronate monomer 1.

We hypothesized that the inefficient participation of Ar-BMIDA monomer 1 in the initial stage of polymerization was due to the first cross-coupling event between the Pd catalytic initiator 4 and the Ar-BMIDA monomer 1 being severely restricted. Given the steric bulk of the MIDA-boronate functional group, we could assume its unfavorable steric repulsion with the *ortho*-tolyl moiety of 4 that might hinder the direct transmetalation step between Ar-BMIDA monomer and the ortho-tolyl-Pd^{II} center. Such steric encumberment would be partially relieved after the first cross-coupling event following the Pd oxidative addition to the C-Br bond of the newly incorporated fluorenyl monomer unit, thus allowing further chain propagation to occur via the less hindered direct Ar-BMIDA transmetalation steps. To support this hypothesis, a phenyl catalytic initiator 5 was prepared and studied in polymerization. A comparative Ag⁺-mediated polymerization was done with this less sterically congested initiator system in similar reaction conditions (entry 9 in Table 1). A PF polymer with an improved M_n 8.53 kDa (\mathcal{D} 1.28) and 41% yield was obtained suggesting a more rapid initiation. Polymerization kinetic experiment yielded a pseudo first-order polymerization rate constant k_{polym} 0.17 h⁻¹ therefore demonstrating a more rapid and uniform initiation (Figure S4 in the Supporting Information). Still, the higher steric bulkiness of MIDA-boronate group would continue lingering over the entire polymerization process as long as the direct BMIDA transmetalation is involved. This steric reasoning could explain the generally lower rate of polymerization of MIDA-boronate monomer 1 compared to the less sterically encumbered boronic acid monomer 2. Overall, this small study suggested that steric hindrance of the aryl moiety at PdII center can lead to inefficient direct Ar-BMIDA transmetalation resulting in delayed polymerization initiation and overall less efficient SCTP.

Impact of the ligand structure. In order to study the impact of phosphine ligand structure on the direct MIDA-boronate transmetalation pathway, some other Pd^{II} catalytic initiators with an *ortho*-tolyl moiety and different Buchwald-type phosphine ligands were synthesized and compared in SCTP conditions with RuPhos catalytic initiator 4 (entry 2 and entries 10-12 in Table 1). With MIDA-boronate monomer 1, each catalytic initiator resulted in PF polymer with values of M_n around 5 kDa but with

noticeable differences in dispersity D. Both the RuPhos and XPhos catalytic initiators $\mathbf{4}$ and $\mathbf{7}$ produced polymers with narrower D values between 1.13-1.16, whereas catalytic initiators with BrettPhos ($\mathbf{6}$) and EPhos ($\mathbf{8}$) ligands produced polymers with broader D values ranging within 1.40-1.41. A major structural difference between the two sets of ligands is in the presence of an alkoxy group attached in the *ortho* position with respect to the Cy₂P substituent in the latter two ligands. The alkoxy group implies a mild electronic effect resulting in increasing overall electron density on the P center that could impact SCTP leading to nonuniformity between growing chains and thus an observed increase in D.

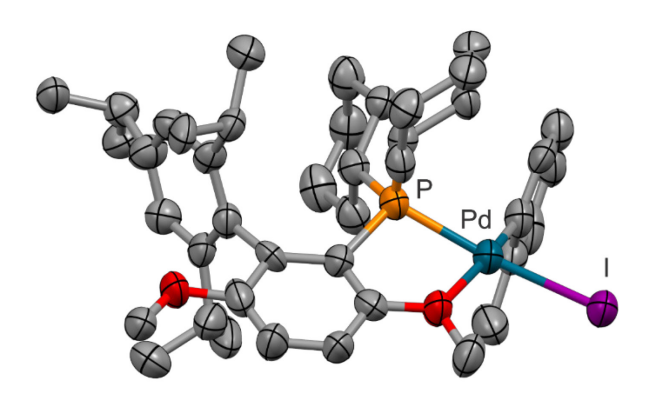


Figure 7. Ellipsoid drawing at the 50% level, representing crystal structure of the O-isomer of Pd^{II}(BrettPhos) catalytic initiator **6**. Hydrogen atoms are omitted for clarity; one of the isopropyl groups was disordered over two positions, with only one position shown.

To gain insight into the mechanistic impact of varying phosphine ligand structure, we carried out polymerization kinetics studies with different catalytic initiators (Figure S1 in the Supporting Information). With BrettPhos catalytic initiator $\mathbf{6}$, a pseudo first-order polymerization rate constant $k_{\text{polym}} 0.068 \, \text{h}^{-1}$ was obtained. This rate was slower than that obtained with the RuPhos catalytic initiator $\mathbf{4}$ but still faster than MIDA-boronate monomer $\mathbf{1}$ hydrolysis rate. Therefore, the direct Ar-BMIDA transmetalation was still operative in SCTP but the overall process was somewhat hindered. Pd complexes with BrettPhos ligand are known to readily isomerize between two coordination isomers: the C-isomer similar to the one formed with the RuPhos ligand and O-isomer (formed through Pd

coordination with O atom of the methoxy group in the *ortho* position with respect to P atom). A pure O-isomer of 6 was isolated via recrystallization, and its structure was confirmed by single-crystal X-ray crystallography (Figure 7). A ³¹P NMR signal at 38.4 ppm was observed after immediate dissolution of this isomer. After 2 h at room temperature, a second signal at 29.5 ppm appeared that could be assigned to the C-isomer, with an approximate isomer ratio of 1:1 (Figure S23 in the Supporting Information). The rate of isomerization was found to be relatively fast compared to the rate of polymerization (an estimated first-order rate constant for the conversion of O-coordinated isomer to C-coordinated isomer was 0.11 h⁻¹). Thus, this demonstrated that both C- and O-coordinated isomers of the Pd^{II}(BrettPhos) complex could likely coexist in equilibrium during SCTP. Previously, Buchwald has proposed that O-isomer of Pd^{II}(BrettPhos) complexes would act as an unreactive "off-cycle" reservoir of Pd catalyst due to the decreased ability of O-isomers to perform reductive elimination.³⁹

To learn more details about the functioning of RuPhos and BrettPhos ligands in SCTP, we carried out a DFT computational study of the various Pd species involved in the process. All computations were done at APFD/6-31G(d,p) level of theory (with def2tzvpp ECP basis set for Pd and I) with PCM solvation treatment (THF); the energy values of the optimized geometries were ZPE and thermal corrected. First, to check the accuracy of the computed geometries of the Pd complexes (and hence the reliability of the obtained energies), we carried out an independent geometry optimization of the O-isomer of BrettPhos catalytic initiator **6**. As can be seen in Figure S8 in the Supporting Information, the computed geometry matched nearly perfectly with the geometry obtained using X-ray crystallography. Then, we proceeded with optimizing geometries of the two Pd⁰(RuPhos) π -complexes formed after initial coupling of the *ortho*-tolyl unit with monomer **1** (and representing two discrete steps in the process of Pd⁰ catalyst migration), and the corresponding Pd^{II} complex resulting from oxidative addition of Pd⁰ to the terminal C–Br bond (Figure 8a). We also carried out computations of the related Pd intermediates with BrettPhos ligand; in this case, we optimized geometry of both C- and O-isomers (Figure 8b, c). In the case of RuPhos ligand, we found that the Pd⁰ migration to the C–Br terminus was

a slightly (1.6 kcal/mol) uphill process, whereas the formation of an oxidative addition Pd^{II} complex was a 19.5 kcal/mol exothermic process (Figure 8a). Overall, the ~20 kcal/mol difference between the oxidative addition complex and the π -complex (which is formed in the reductive elimination step) would put the overall polymerization process within the realm of the possible thermally activated reactions.

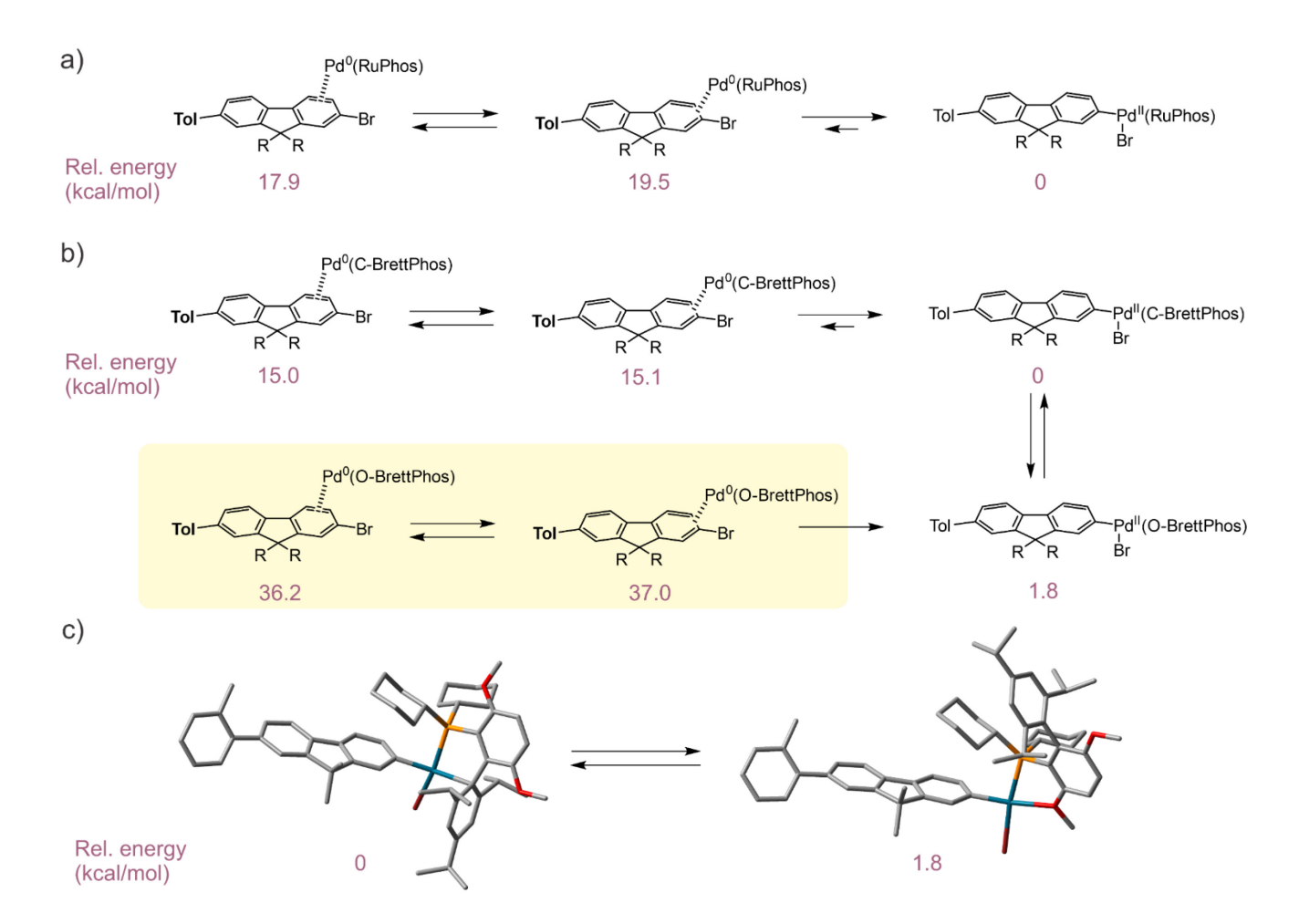


Figure 8. Computational studies of the Pd⁰ and Pd^{II} complexes with RuPhos (a) and BrettPhos (b) ligands involved in the SCTP process. In the case of BrettPhos ligand, C-BrettPhos and O-BrettPhos refer to C- and O-isomers, respectively. c) Optimized geometries of the C- and O-isomers of Pd^{II}(BrettPhos) oxidative addition complexes. All computations were performed at APFD/6-31G(d,p) level of theory (with def2tzvpp ECP basis set for Pd) with PCM solvation treatment (THF); the energy values of the optimized geometries were ZPE and thermal corrected. For better computational efficiency, octyl side groups at the fluorenyl moiety were replaced with methyl groups.

The situation with BrettPhos ligand was more complicated. The energies of Pd^{II} complexes resulting from oxidative addition to the terminal C-Br bond for C- and O-coordinated isomers were

within 1.8 kcal/mol of each other, thus reflecting the existence of the equilibrium between these two complexes (Figure 8c). In the case of C-isomer, the corresponding Pd^0 π -complexes were about 15 kcal/mol higher in energy than the C-isomer of Pd^{II} oxidative addition complex (Figure 8b). This was similar to the situation with Pd-RuPhos complexes. In contrast, the energy of the O-isomer Pd^0 π -complexes was about 35 kcal/mol higher relative to the energy of the corresponding Pd^{II} complex. Such a high energy would make formation of the O-isomer π -complexes too prohibitive in the thermal reaction conditions, and therefore would result in severely hindered reductive elimination step from the O-isomer Pd^{II} (BrettPhos) complexes. This confirmed that O-complexes would be unreactive in SCTP conditions. Despite the unreactivity of the O-isomer, the fast equilibrium between the C- and O-coordinated isomers would minimize the negative impact of the presence of O-isomer on the overall polymerization rate, in agreement with our polymerization kinetic data.

We also addressed the higher dispersity of PF polymer produced in polymerization with BrettPhos catalytic initiator **6**. The broader D values could be due to more facile dissociation of the Pd⁰ center from the corresponding π -complexes during a catalyst-transfer step, resulting from the lower binding energy in the π -complex. The bonding structure of a Pd⁰ π -complex could be described in terms of the Dewar-Chatt-Duncanson model, ⁴⁰ where the two primary contributors are donor-acceptor bonding interactions between Pd 4d lone pair and aromatic π * MO, and aromatic π MO and Pd 5s vacant orbital. To estimate the energies of these interactions, we carried out Natural Bond Orbital (NBO) analysis on the geometry-optimized π -complexes (Table 2 and Figure S9 in the Supporting Information). The NBO method transforms a delocalized many-electron molecular wavefunction into localized electron-pair orbitals that could be assigned to specific MO interactions of interest. ⁴¹ The energies of the contributing bonding MO interactions were estimated from the second-order perturbation theory analysis of the Fock matrices in NBO basis. The results in Table 2 show about a 13 kcal/mol lower binding energy in the reactive C-coordinated isomer of Pd⁰(BrettPhos) complex (as compared to the corresponding Pd⁰(RuPhos) complex). The lower binding energy might be attributed to the elevated

steric bulkiness of the BrettPhos ligand. This could explain the higher Pd^0 (BrettPhos) dissociation propensity and hence higher D values in the case of SCTP catalyzed by the catalytic initiator $\mathbf{6}$. It is also interesting to note a significantly higher Pd^0 binding energy of the unreactive O-coordinated Pd^0 (BrettPhos) isomer. Such a high π -binding energy could additionally preclude Pd catalyst transfer thus further contributing to the low reactivity of the O-coordinated Pd-BrettPhos complexes in SCTP process.

Table 2. NBO analysis of the energy of bonding interactions in the Pd⁰ π -complexes (in kcal/mol). ^a

MO interaction	Pd ⁰ (RuPhos)	Pd ⁰ (C-BrettPhos)	Pd ⁰ (O-BrettPhos)
$4d$ lone pair Pd \rightarrow arom. π^*	40.2	31.9	51.1
Arom. $\pi \rightarrow 5s$ Pd	20.6	15.6	48.4
Total binding energy	60.8	47.5	99.5

^a NBO analysis was done on the structures geometry optimized at APFD/6-31G(d,p) level of theory (def2tzvpp basis set for Pd) with PCM solvation treatment (THF).

To mitigate the negative effect of equilibrating C- and O-isomers on cross-coupling outcome, the ligand EPhos has been introduced for the use in Buchwald-Hartwig amination. 42,43 Due to the added steric bulk at the coordinating O atom, Pd-EPhos complexes exist predominantly in the form of C-isomer. Therefore, using EPhos ligand could help to experimentally evaluate the role of equilibrating C- and O-coordinated isomers in the case of BrettPhos complexes. For this purpose, we prepared EPhos catalytic initiator **8** (Figure 2b). ³¹P NMR spectrum of **8** at room temperature in a CD₂Cl₂ solution showed predominantly one resonance signal at 30.6 ppm with another low intensity signal at 37.2 ppm (Figure S27 in the Supporting Information). The dominating ³¹P resonance was attributed to the C-isomer given its upfield NMR shift relative to the other signal; the integration of the two signals gave about 95% of the C-isomer. A kinetic study (Figure S1 in the Supporting Information) found a pseudo first-order polymerization rate similar to the BrettPhos systems (*k*_{polym} 0.065 h⁻¹). Assuming the

similarity in polymerization kinetics for EPhos and BrettPhos Pd complexes, the C-isomer was assigned as the active catalytic species, thus confirming the results obtained in the computational study. Therefore, the observed decrease in polymerization rate relative to Pd-RuPhos system was hypothesized to be related to the sterically hindered direct MIDA-boronate transmetalation step that should be a rate-determining step in the SCTP process. The increased steric hindrance of BrettPhos and EPhos ligands could stem from the three isopropyl groups on the second ("lower") phenyl ring of these two ligands.

Polymerization "critical length" and ambivalence of the "living" character. information on the SCTP of monomers 1 and 2 was obtained upon analysis of MALDI-TOF mass spectral data for the resulting PF polymers. The mass spectral analysis is used to evaluate end-group composition of the polymers and can provide some useful hints about the polymerization mechanism. Assuming the controlled chain-growth mechanism, a living polymer chain should be terminated with an ortho-tolyl group (from the catalytic initiator 4) on one chain end, and with a Pd(L)Br unit on the other chain end (where L is a phosphine ligand, e.g. RuPhos in the case of catalytic initiator 4).²² The latter unit could be replaced with H or Br as a result of an acidic post-polymerization workup. Such polymers will be referred to as $Tol-(PF)_n-Pd(L)Br$, $Tol-(PF)_n-H$ or $Tol-(PF)_n-Br$, respectively. For our studies, we used a relatively mild post-polymerization workup involving adding 6 M HCl to the reaction and stirring the resulting mixture at 45 °C for 1 h. MALDI-TOF mass spectrum of a polymer prepared from boronic acid monomer 2 using an M₀/I₀ feed ratio 24 (entry 3 in Table 1) displayed a dual molecular weight distribution (Figure 9a). A component with lower molecular weight was characterized by Tol-(PF)_n-H and Tol-(PF)_n-Br molecular compositions. A larger molecular weight component consisted predominantly of Tol-(PF)_n-Pd(L)⁺ along with matching Tol-(PF)_n-H or Tol-(PF)_n-Br molecular compositions. Since MALDI ionization likely resulted in the loss of halide anion, the initial composition of the Pd-terminated chains was Tol-(PF)_n-Pd(L)Br. The presence of these two distinct distributions was responsible for a relatively high dispersity of this polymer sample (D 1.43). Detection of the Pd^{II} terminated chains reflects the relatively good stabilization by the Buchwald-type phosphine ligands of the Pd(L)Br end-groups in mild acidic conditions, and was observed previously by us.²² An acid-promoted removal of the active Pd^{II} center would result in Tol–(PF)_n–H chains (Figure 10). The presence of a matching set of Tol–(PF)_n–Br polymer chains could be explained by an equilibrium between the Pd⁰ π -complex and Pd^{II} complex, with the former responsible for Br chain termination (such an equilibrium would be feasible considering the ~20 kcal/mol calculated energy difference between the oxidative addition Pd^{II}(RuPhos) complex and the Pd⁰(RuPhos) π -complex, *vide supra*). Thus, both smaller and larger molecular weight components detected in the MALDI-TOF mass spectra originated from the formally living chains containing either Pd⁰ or Pd^{II} groups. Assuming that removal of Pd during acidic post-polymerization treatment would be more facile from a Pd⁰ π -complex, the absence of detectable Pd-terminated chains in the lower molecular weight component might reflect the predominance of Pd⁰ π -complex prior to the quenching. In contrast, the higher molecular weight component was dominated by the active Pd^{II}(L)Br end-group complex.

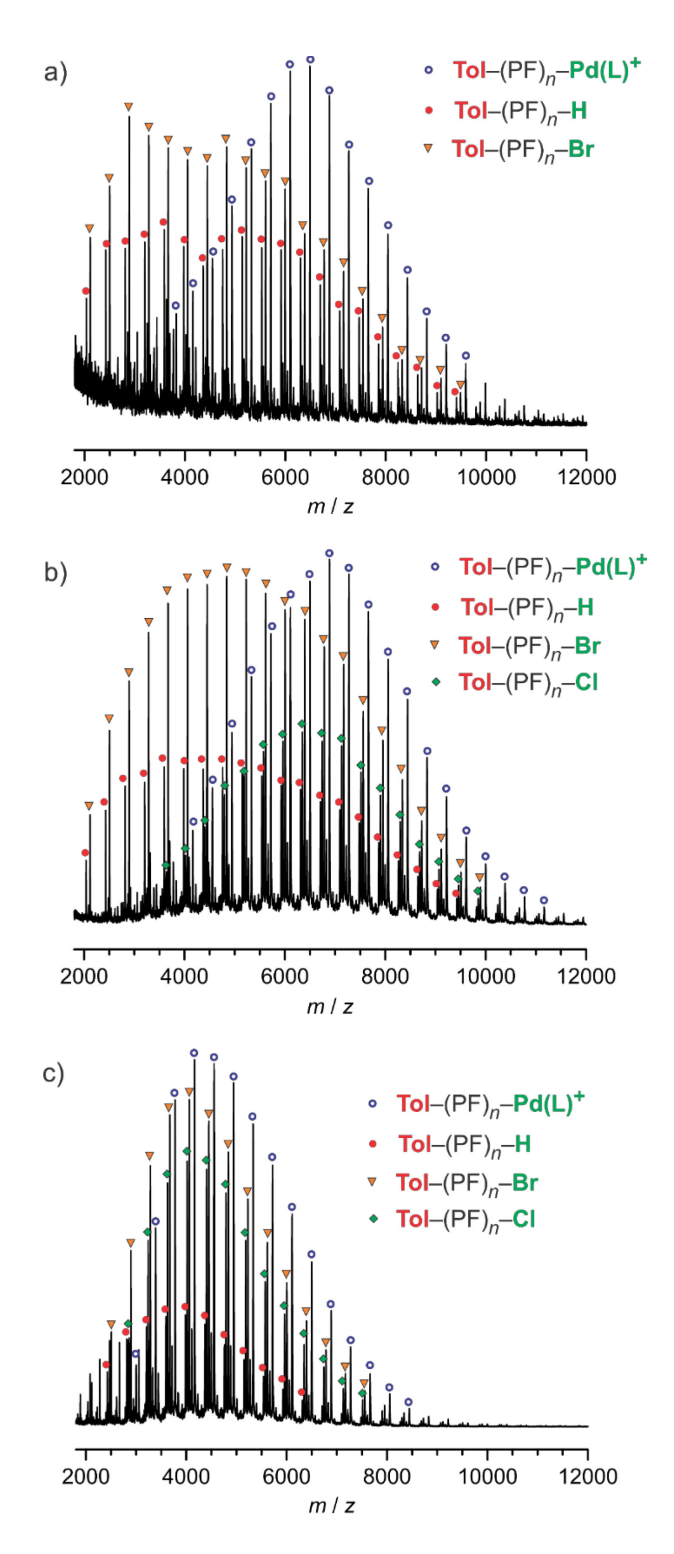


Figure 9. MALDI-TOF mass spectra for the PF polymer produced in SCTP of boronic acid monomer **2** using M_0/I_0 ratio 24:1 in the conditions of varying MIDA content: a) no MIDA (entry 3 in Table 1), b) 1 eq. of MIDA (entry 4 in Table 1), and c) 3 eq. of MIDA (entry 5 in Table 1). The chain composition corresponding to specific peaks is marked with colored symbols, L is RuPhos.

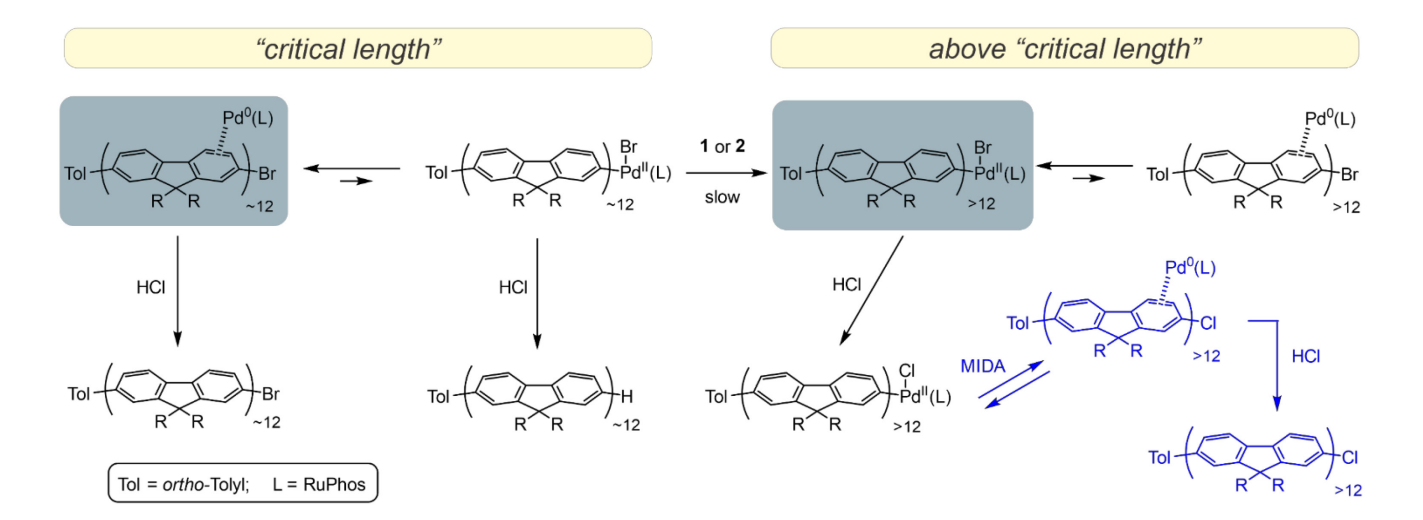


Figure 10. Schematic interpretation of the experimentally found polymer end-group composition, and illustration of the "critical length" concept. Blue rectangles indicate preferred structure at the polymer "critical length", and above the "critical length". The reaction route shown in blue is facilitated in the presence of MIDA.

The presence of the two distinct molecular weight distributions reflected two different kinetic regimes of the polymerization. The lower molecular weight distribution resulted from a slow polymerization which nearly stopped once the polymer chain reached a certain "critical length" (of about 12 fluorenyl repeat units). On the other hand, the larger molecular weight component resulted from an active propagation which continued until consumption of all the available monomer 2. Further support for the involvement of the two polymerization regimes was provided by analysis of the PF polymer produced in the polymerization of monomer 2 using M_0/I_0 ratio 36:1 (entry 18 in Table 1). MALDITOF mass spectral data on this sample indicated a similar dual molecular weight distribution, with the lower molecular weight domain displaying $Tol-(PF)_n$ —H and $Tol-(PF)_n$ —Br chain composition with a similar molecular weight as in the case of PF obtained using the M_0/I_0 ratio 24:1 (Figure S10 in the Supporting Information). In contrast, the higher molecular weight domain displayed predominantly $Tol-(PF)_n$ —Pd(L)Br chain composition (a rather small intensity of the higher molecular weight peaks was not indicative of its smaller abundance but was due to a reduced sensitivity of the MALDI-TOF spectrometer toward the higher molecular weight polymer chains). The larger difference between

molecular weights of the two components resulted in the higher overall dispersity (D 1.54) compared to the polymer obtained at a lower M_0/I_0 ratio. The bimodal molecular weight distribution could be also observed on the GPC traces from the polymers obtained at the varying M_0/I_0 feed ratio (Figure S11 in the Supporting Information). A lower molecular weight band, that was exclusively found at M_0/I_0 12:1, was retained in the samples of the polymers obtained at the higher M_0/I_0 ratio values, whereas the second, higher molecular weight band was shifting towards the higher molecular weights. Thus, it appears that one component (consisting mostly of Pd^{II} terminated chains) exhibited an efficient controlled polymerization whereas the other, lower molecular weight component was characterized by a stagnated polymerization below the "critical length". Since weight average molecular weight M_w is more reflective of the higher molecular weight component, it exhibited an expected nearly linear dependence on the M_0/I_0 ratio within the studied range (Figure 11). The M_n , on the other hand, exhibited a more stagnated behavior upon an increasing M_0/I_0 ratio, leading to the increasing dispersity D of the polymer samples obtained at the higher M_0/I_0 values.

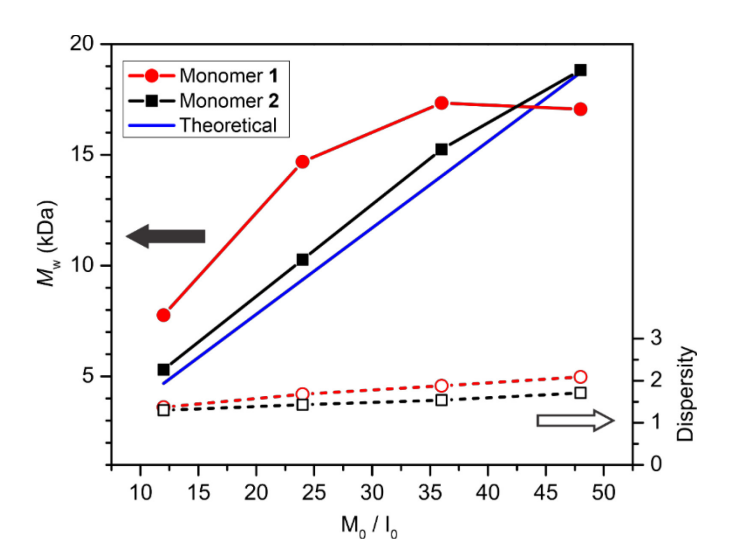


Figure 11. Control of polymer molecular weight via variation of the M_0/I_0 feed ratio. The polymerizations were done using catalytic initiator **4**, in Ag^+ -mediated conditions for monomer **1**, and without added Ag^+ for monomer **2**.

To explain the two distinct polymerization regimes simultaneously occurring in the SCTP of boronic acid monomer **2**, we hypothesized that since Pd^0 migration across the conjugated PF chain could be a random walk process (by analogy with the previously demonstrated Ni^0 random walk in Kumada catalyst-transfer polymerization^{44, 45}), it is limited by the "critical length" of about 12 fluorenyl repeat units. Whether there are kinetic or thermodynamic stability factors responsible for this, the Pd^0 gets essentially entrapped as a π -complex within a "critical length" fragment, which dramatically inhibits further polymerization and results in the persistence of "living" (from the standpoint of possessing a Pd center) but barely polymerizable chains. Such "critical length" chains are formed first in the polymerization process. Upon acid post-polymerization quenching, they would yield the lower molecular weight polymer distribution. In contrast, with extended polymerization time, once a Pd center overcomes the favorable Pd^0 "critical length" complex, it would become predominantly a truly living reactive Pd^{II} end-group complex capable of efficient chain propagation and sustaining controlled polymerization. Although this simple hypothesis can explain the experimental observation, further investigations are needed to prove it (or support an alternative explanation).

Since we demonstrated that presence of MIDA hinders polymerization of boronic acid monomer 2, we studied MALDI-TOF mass spectra of the PF samples obtained upon polymerization of 2 in the presence of 1 and 3 eq. of MIDA. The presence of the dual molecular weight distribution was still noticeable in the case of polymerization with 1 eq. of MIDA (Figure 9b). One noticeable difference was a clear presence of the Tol–(PF) $_n$ –Cl chain composition in the higher molecular weight distribution component. Formation of such chains would be possible in the process of HCl post-polymerization quenching of the living polymer chains upon enforcing a reversible and energetically favorable equilibrium between Pd^{II} end-group complex and Pd⁰ π -complex (Figure 10). As we discussed above, MIDA can possibly interact with a Pd⁰ complex and hence facilitate the equilibrium shift toward a Pd⁰ π -complex. The MIDA-enforced higher prevalence of the unreactive Pd⁰ π -complex would decrease the availability of the reactive Pd^{II} complex and therefore would interfere with subsequent

transmetalation and slow down the polymerization process (in agreement with the "critical length" hypothesis above). The MALDI-TOF mass spectral data for the polymerization in the presence of 3 eq. of MIDA (Figure 9c) showed a single molecular weight distribution with even more intense signals from the Tol–(PF)_n–Cl chain composition. This indicated a further MIDA-enforced Pd^{II} – Pd⁰ complex equilibrium favoring a Pd⁰ π -complex leading to essential stagnation of the polymerization process once the "critical length" has been reached.

A generally similar behavior was observed with the MIDA-boronate monomer 1 polymerization in Ag⁺-mediated conditions. The polymerization using catalytic initiator 4 was carried out for 40 h (to account for a slower polymerization rate with MIDA-boronate monomer 1) and afforded a reasonable molecular weight control (with respect to $M_{\rm w}$) up to M_0/I_0 feed ratio of 36 (Figure 11). MALDI-TOF mass spectra of the PF polymer obtained using M_0/I_0 feed ratio of 24 (entry 14 in Table 1) also displayed two molecular weight distributions with the dominating $Tol-(PF)_n$ -H and $Tol-(PF)_n$ -Br chain compositions, along with $Tol-(PF)_n-Pd(L)^+$ (Figure 12a). These two molecular weight distributions generally matched the two distributions obtained at the same M_0/I_0 ratio using boronic acid monomer 2. The lower molecular weight distribution corresponded to a similar "critical length" (of about 12 fluorenyl repeat units) and was likely formed first followed by the formation of a higher molecular weight distribution component. The GPC traces of the polymers obtained upon the varying M_0/I_0 feed ratios similarly exhibited dual band distribution (Figure S12 in the Supporting Information). Because of the slower polymerization rate with monomer 1, the formation of the lower molecular weight distribution happened within the first 24 h of polymerization. Indeed, a sample of the polymer obtained after HCl quenching of the polymerization reaction after 24 h revealed a predominant lower molecular weight distribution in the MALDI-TOF mass spectrum (Figure 12b). The less efficient molecular weight control in the case of MIDA-boronate monomer 1 (as compared to boronic acid monomer 2) could be related both to the slower rate of polymerization involving MIDA-boronate monomer and to the delayed reaction initiation due to elevated steric hindrance imposed by the bulky MIDA-boronate moiety in monomer 1 at the direct transmetalation step.

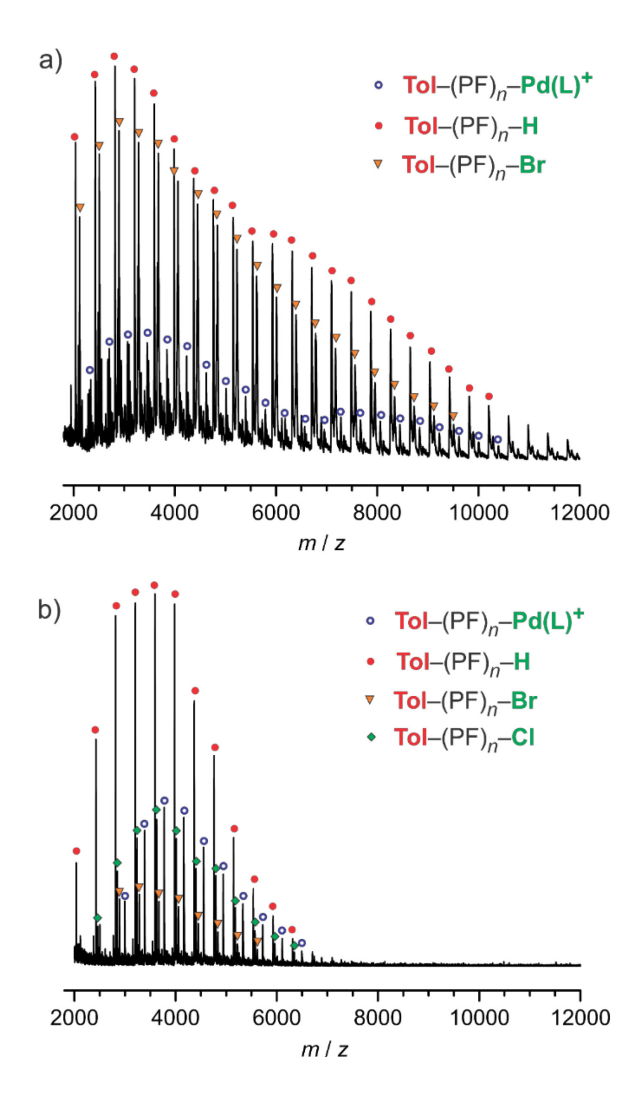


Figure 12. MALDI-TOF mass spectra for the PF polymer produced in SCTP of MIDA-boronate monomer **2** using the M_0/I_0 feed ratio 24:1 in the Ag^+ -mediated conditions: a) sample after 40 h polymerization time (entry 14 in Table 1), b) sample after 24 h polymerization time. The chain composition corresponding to specific peaks is marked with colored symbols, L is RuPhos.

The "critical length" phenomenon was also observed for the Ag^+ -mediated polymerization of the MIDA-boronate monomer 1 with the phenyl catalytic initiator 5 that demonstrated a more efficient SCTP due to the more rapid and uniform initiation step (*vide supra*). When the polymerization was done using M_0/I_0 feed ratio of 24 (entry 9 in Table 1), the MALDI-TOF mass spectral data on a sample

obtained early in the polymerization process (after 11 h polymerization time) showed a single molecular weight distribution matching the "critical length" observed in the previous runs (Figure S14a in the Supporting Information). The dominating chain compositions (Ph–(PF) $_n$ –H, Ph–(PF) $_n$ –Br, and Ph–(PF) $_n$ –Pd(L) $^+$, where L is RuPhos) reflected controlled character of the polymerization at this stage. A sample obtained upon longer polymerization time (after 22 h polymerization) exhibited a bimodal molecular weight distribution with a higher molecular weight component along with a lower molecular weight "critical length" component (Figure S14b in the Supporting Information). Interestingly, the lower molecular weight component was dominated by the Ph–(PF) $_n$ –Br chain composition, whereas the higher molecular weight component showed a predominant Ph–(PF) $_n$ –H chain composition. This likely reflected the "entrapment" of the Pd 0 π -complex within a "critical length" fragment, hindering the polymerization and yielding the dominating Ph–(PF) $_n$ –Br chain composition upon acid post-polymerization quenching. Overall, this provided an additional support for the "critical length" concept.

We also investigated *ortho*-tolyl Pd BrettPhos and XPhos catalytic initiators 6 and 7 in the polymerization of MIDA-boronate monomer 1 in Ag⁺-mediated conditions. The polymerizations were carried out at different M_0/I_0 feed ratios for the total 40 h reaction time. We found that the BrettPhos system displayed a linear increase of M_w with respect to increasing M_0/I_0 ratio but the molecular weight remained well below the theoretical values even with extended reaction time (Figure S13 in the Supporting Information). The less effective polymerization control could be due to an essentially suppressed ability of the active Pd center to overcome the "critical length" restriction. The MALDI-TOF data of the polymer obtained at M_0/I_0 ratio of 24 indicated a dual molecular weight distribution similar to the one obtained for the case with Pd-RuPhos catalytic initiator 4. The higher molecular weight distribution, in addition to dominating $Tol-(PF)_n$ -Pd(L)⁺ chain composition, contained an intense set of peaks corresponding to $Tol-(PF)_n$ -Cl chain compositions (Figure S15 in the Supporting Information). As such composition is indicative of the facile Pd^{II} -Pd⁰ equilibrium with the Pd^0 π -complex domination, it indeed pointed on the inefficient chain propagation beyond the "critical length"

of the polymer chain. In addition, there was a prominent set of peaks corresponding to a BMIDA– $(PF)_n$ – $Pd(L)^+$ chain composition, which indicated a Pd^0 intermolecular transfer to a monomer 1 with subsequent oxidative addition to the C–Br bond of 1 and initiation of a new polymer chain. This undesirable chain-transfer process stemmed from a lower binding energy in the Pd^0 (BrettPhos) π -complex, in agreement with our computational NBO analysis described above.

The XPhos system showed even less control, with $M_{\rm w}$ nearly stagnating at around 4-5 kDa independent on the M_0/I_0 feed ratios (Figure S13 in the Supporting Information). The chain end-group composition in that case was complex, with noticeable $Tol-(PF)_n-Pd(L)^+$, $Tol-(PF)_n-Cl$, $Tol-(PF)_n-Br$, and Tol-(PF)_n-H sets within a single molecular weight distribution corresponding to the "critical length" (Figure S16 in the Supporting Information). As all the molecular compositions detected in the mass spectral data reflected the exclusive presence of the "living" chains (in a sense of each chain having an associated Pd center), the lack of molecular weight control reflected the inability of the Pd-XPhos center (existing predominantly as a Pd⁰ π -complex) to overcome the "critical length" restriction and continue the polymerization. Overall, these results painted a sophisticated picture of the SCTP process with MIDA-boronate monomers where the mere presence of a Pd center on the polymer chain was not sufficient to sustain the polymerization (even if a chain could be considered "living" in the sense of possessing a Pd center), and the choice of phosphine ligand on the Pd center was a critical tool to overcome the "critical length" restriction. We assume that these findings can be applied to other cases of monomers less reactive in SCTP, where broad dispersities and less efficient molecular weight control were observed even with seemingly "living" character of the polymerization.⁴⁶

Conclusions

Aryl and heteroaryl MIDA-boronates remain a promising class of monomers for controlled SCTP. They are particularly efficient for polymerizations involving heteroaromatic systems (such as thiophenes). However, our work has uncovered a major limitation of MIDA-boronates in the case of

less reactive fluorenyl (and potentially other all-carbon aromatic systems) monomers that is related to

the inhibiting effect of free MIDA byproduct formed in the polymerization. This inhibiting effect

originates from MIDA's interaction with Pd⁰ centers during the chain-growth polymerization. The

beneficial role of added Ag⁺ is that it facilitates removal of free MIDA through the formation of an

insoluble precipitate. However, in Ag⁺-mediated polymerization conditions, a key mechanistic step –

transmetalation - occurs as a direct interaction between MIDA-boronate and the chain-end hydroxo-

Pd^{II} complex and therefore suffers from steric bulkiness of the MIDA-boronate group, especially at the

initiation step. These complications could diminish the synthetic value of MIDA-boronate monomers

in SCTP, although better understanding of these implications and a proper choice of polymerization

conditions and catalytic initiators could to some extent mitigate such problems. As part of this project,

we also uncovered a "critical length" phenomenon which results in a dual molecular weight distribution

of the produced PF polymer, both with MIDA-boronate and boronic acid monomers. The generality of

this phenomenon and whether it is restricted to using Pd catalytic systems based on Buchwald-type

phosphine ligands remains to be studied, however, a proper choice of the phosphine ligand could help

to overcome the "critical length" limitation.

Supporting Information Available. Detailed synthetic and experimental procedures, and additional

data and figures. This material is available free of charge via the Internet at http://pubs.acs.org.

Corresponding Author

E-mail: een@niu.edu (E.E.N.).

Notes

The authors declare no competing financial interest.

Acknowledgements. This research was supported by the U.S. National Science Foundation (NSF)

under the grant CHE-2004117. Purchase of the NMR spectrometer used to obtain results included in

34

this publication was supported by the NSF under the MRI award CHE-2117776. This work used resources of the Center for Research Computing and Data at Northern Illinois University. We thank Dr. Fabrizio Donnarumma (Louisiana State University) for assistance with acquiring MALDI-TOF data.

References:

- (1) Guo, X.; Facchetti, A. The journey of conducting polymers from discover to application. *Nat. Mater.* **2020**, *19*, 922-928.
- (2) Swager, T. M. *50th anniversary perspective:* conducting/semiconducting conjugated polymers. A personal perspective on the past and the future. *Macromolecules* **2017**, *50*, 4867-4886.
- (3) Nezakati, T.; Seifalian, A.; Tan, A.; Seifalian, A. M. Conductive polymers: opportunities and challenges in biomedical applications. *Chem. Rev.* **2018**, *118*, 6766-6843.
- (4) Tran, V. V.; Lee, S.; Lee, D.; Le, T.-H. Recent developments and implementations of conductive polymer-based flexible devices in sensing applications. *Polymers* **2022**, *14*, 3730.
- (5) Yokozawa, T.; Ohta, Y. Scope of controlled synthesis *via* chain-growth condensation polymerization: from aromatic polyamides to π -conjugated polymers. *Chem. Commun.* **2013**, *49*, 8281-8310.
- (6) Leone, A. K.; Mueller, E. A.; McNeil, A. J. The history of palladium-catalyzed cross-couplings should inspire the future of catalyst-transfer polymerization. *J. Am. Chem. Soc.* **2018**, *140*, 15126-15139.
- (7) Mayhugh, A. L.; Yadav, P.; Luscombe, C. K. Circular discovery in small molecule and conjugated polymer synthetic methodology. *J. Am. Chem. Soc.* **2022**, *144*, 6123-6135.

- (8) Yokoyama, A.; Suzuki, H.; Kubota, Y.; Ohuchi, K.; Higashimura, H.; Yokozawa, T. Chain-growth polymerization for the synthesis of polyfluorene via Suzuki-Miyaura reaction from an externally added initiator unit. *J. Am. Chem. Soc.* **2007**, *129*, 7236-7237.
- (9) Sun, H.; Zhang, S.; Yang, Y.; Li, X.; Zhan, H.; Cheng, Y. Excellent control of perylene diimide end group in polyfluorene via Suzuki catalyst transfer polymerization. *Macromol. Chem. Phys.* **2016**, *217*, 2726-2735.
- (10) Bautista, M. V.; Varni, A. J.; Ayuso-Carrillo, J.; Tsai, C.-H.; Noonan, K. J. T. Chain-growth polymerization of benzotriazole using Suzuki-Miyaura cross-coupling and dialkylbiarylphosphine palladium catalysts. *ACS Macro Lett.* **2020**, *9*, 1357-1362.
- (11) Tokita, Y.; Katoh, M.; Kosaka, K.; Ohta, Y.; Yokozawa, T. Precision synthesis of a fluorene-thiophene alternating copolymer by means of the Suzuki-Miyaura catalyst-transfer condensation polymerization: the importance of the position of an alkyl substituent on thiophene of the biaryl monomer to suppress disproportionation. *Polym. Chem.* **2021**, *12*, 7065-7072.
- (12) Lee, J.; Ryu, H.; Park, S.; Cho, M.; Choi, T.-L. Living Suzuki-Miyaura catalyst-transfer polymerization for precision synthesis of length-controlled armchair graphene nanoribbons and their block copolymers. *J. Am. Chem. Soc.* **2023**, *145*, 15488-15495.
- (13) Beryozkina, T.; Boyko, K.; Khanduyeva, N.; Senkovskyy, V.; Horecha, M.; Oertel, U.; Simon, F.; Stamm, M.; Kiriy, A. Grafting of polyfluorene by surface-initiated Suzuki polycondensation.
 Angew. Chem. Int. Ed. 2009, 48, 2695-2698.
- (14) Carrillo, J. A.; Ingleson, M. J.; Turner, M. L. Thienyl MIDA boronate esters as highly effective monomers for Suzuki-Miyaura polymerization reactions. *Macromolecules* **2015**, 48, 979-986.

- (15) Seo, K.-B.; Lee, I.-H.; Lee, J.; Choi, I.; Choi, T.-L. A rational design of highly controlled Suzuki-Miyaura catalyst-transfer polycondensation for precision synthesis of polythiophenes and their block copolymers: marriage of palladacycle precatalysts with MIDA-boronates. *J. Am. Chem. Soc.* **2018**, *140*, 4335-4343.
- (16) Lee, J.; Park, H.; Hwang, S.-H.; Lee, I.-H.; Choi, T.-L. RuPhos Pd precatalyst and MIDA boronate as an effective combination for the precision synthesis of poly(3-hexylthiophene): systematic investigation of the effect of boronates, halides, and ligands. *Macromolecules* **2020**, *53*, 3306-3314.
- (17) Lee, J.; Kim, H.; Park, H.; Kim, T.; Hwang, S.-H.; Seo, D.; Chung, T. D.; Choi, T.-L. Universal Suzuki-Miyaura catalyst-transfer polymerization for precision synthesis of strong donor/acceptor-based conjugated polymers and their sequence engineering. *J. Am. Chem. Soc.* **2021**, *143*, 11180-11190.
- (18) Kim, H.; Lee, J.; Kim, T.; Cho, M.; Choi, T.-L. Precision synthesis of various low-bandgap donor-acceptor alternating conjugated polymers via living Suzuki-Miyaura catalyst-transfer polymerization. *Angew. Chem. Int. Ed.* **2022**, *61*, e202205828.
- (19) He, C.; Dong, J.; Xu, C.; Pan, X. N-Coordinated organoboron in polymer synthesis and material science. *ACS Polym. Au* **2023**, *3*, 5-27.
- (20) Park, H.; Lee, J.; Hwang, S.-H.; Kim, D.; Hong, S. H.; Choi, T.-L. Modulating the rate of controlled Suzuki-Miyaura catalyst-transfer polymerization by boronate tuning. *Macromolecules* **2022**, *55*, 3476-3483.
- (21) Choi, H.-N.; Yang, H.-S.; Chae, J.-H.; Choi, T.-L.; Lee, I.-H. Synthesis of conjugated rod-coil block copolymers by RuPhos Pd-catalyzed Suzuki-Miyaura catalyst-transfer polycondensation: initiation from coil polymers. *Macromolecules* **2020**, *53*, 5497-5503.

- (22) Howell, M. T.; Kei, P.; Anokhin, M. V.; Losovyj, Y.; Fronczek, F. R.; Nesterov, E. E. Suzuki-Miyaura catalyst-transfer polymerization: new mechanistic insights. *Polym. Chem.* **2023**, 14, 4319-4337.
- (23) Neher, D. Polyfluorene homopolymers: conjugated liquid-crystalline polymers for bright blue emission and polarized electroluminescence. *Macromol. Rapid Commun.* **2001**, *22*, 1365-1385.
- (24) Beaupré, S.; Boudreault, P.-L. T.; Leclerc, M. Solar-energy production and energy-efficient lighting: photovoltaic devices and white-light-emitting diodes using poly(2,7-fluorene), poly(2,7-carbazole), and poly(2,7-dibenzosilole) derivatives. *Adv. Mater.* **2010**, *22*, E6-E27.
- (25) Bernius, M. T.; Inbasekaran, M.; O'Brien, J.; Wu, W. Progress with light-emitting polymers. *Adv. Mater.* **2000**, *12*, 1737-1750.
- (26) Scherf, U.; List, E. J. W. Semiconducting polyfluorenes towards reliable structure-property relationships. *Adv. Mater.* **2002**, *14*, 477-487.
- (27) King, R. P.; Krska, S. W.; Buchwald, S. L. A neophile palladacycle as an air- and thermally stable precursor to oxidative addition complexes. *Org. Lett.* **2021**, *23*, 7927-7932.
- (28) Gonzales, J. A.; Ogba, O. M.; Morehouse, G. F.; Rosson, N.; Houk, K. N.; Leach, A. G.; Cheong, P.H.-Y.; Burke, M. D.; Lloyd-Jones, G. C. MIDA boronates are hydrolyzed fast and slow by two different mechanisms. *Nat. Chem.* **2016**, *8*, 1067-1075.
- (29) Cox, P. A.; Reid, M.; Leach, A. G.; Campbell, A. D.; King, E. J.; Lloyd-Jones, G. C. Base-catalyzed aryl-B(OH)₂ protodeboronation revisited: from concerted proton transfer to liberation of a transient aryl anion. *J. Am. Chem. Soc.* **2017**, *139*, 13156-13165.

- (30) Hayes, H. L. D.; Wei, R.; Assante, M.; Geogheghan, K. J.; Jin, N.; Tomasi, S.; Noonan, G.; Leach, A. G.; Lloyd-Jones, G. C. Prodeboronation of (hetero)arylboronic esters: direct versus prehydrolytic pathways and self-/auto-catalysis. *J. Am. Chem. Soc.* **2021**, *143*, 14814-14826.
- (31) Smrečki, N.; Kukovec, B.-M.; Jaźwiński, J.; Liu, Y.; Zhang, J.; Mikecin, A.-M.; Popović, Z. Preparation and characterization of palladium(II) complexes with *N*-arylalkyliminodiacetic acids. Catalytic activity of complexes in methoxycarbonylation of iodobenzene. *J. Organomet. Chem.* **2014**, *760*, 224-230.
- (32) Smrečki, N.; Kukovec, B.-M.; Rotim, K.; Oršolić, D.; Jović, O.; Rončević, T.; Mužinić, N. R.; Vinković, M.; Popović, Z. Palladium(II) complexes with *N*-alkyliminodiacetic acid derivatives: preparation, structural and spectroscopic studies. *Inorg. Chim. Acta* **2017**, *462*, 64-74.
- (33) Moreno-Mañas, M.; Pérez, M.; Pleixats, R. Palladium-catalyzed Suzuki-type self-coupling of arylboronic acids. A mechanistic study. *J. Org. Chem.* **1996**, *61*, 2346-2351.
- (34) Vasconcelos, S. N. S.; Reis, J. S.; de Oliveira, I. M.; Balfour, M. N.; Stefani, H. A. Synthesis of symmetrical biaryl compounds by homocoupling reaction. *Tetrahedron* **2019**, *75*, 1865-1959.
- (35) Qiu, Y.; Worch, J. C.; Fortney, A.; Gayathri, C.; Gil, R. R.; Noonan, K. J. T. Nickel-catalyzed Suzuki polycondensation for controlled synthesis of ester-functionalized conjugated polymers.

 *Macromolecules** 2016, 49, 4757-4762.
- (36) Sugita, H.; Kamigawara, T.; Miyazaki, S.; Shimada, R.; Katoh, T.; Ohta, Y.; Yokozawa, T. Intramolecular palladium catalyst transfer on benzoheterodiazoles as acceptor monomers and discovery of catalyst transfer inhibitors. *Chem. Eur. J.* **2023**, *29*, e202301242.
- (37) Leone, A. K.; Goldberg, P. K.; McNeil, A. J. Ring-walking in catalyst-transfer polymerization. *J. Am. Chem. Soc.* **2018**, *140*, 7846-7850.

- (38) Fors, B. P.; Watson, D. A.; Biscoe, M. R.; Buchwald, S. L. A highly active catalyst for Pd-catalyzed amination reactions: cross-coupling reactions using aryl mesylates and the highly selective monoarylation of primary amines using aryl chlorides. *J. Am. Chem. Soc.* **2008**, *130*, 13552-13554.
- (39) Arrechea, P. L.; Buchwald, S. L. Biaryl phosphine based Pd(II) amido complexes: the effect of ligand structure on reductive elimination. *J. Am. Chem. Soc.* **2016**, *138*, 12486-12493.
- (40) Mingos, D. M. P. A historical perspective on Dewar's landmark contribution to organometallic chemistry. *J. Organomet. Chem.* **2001**, *635*, 1-8.
- (41) Reed, A. E.; Curtiss, L. A.; Weinhold, F. Intermolecular interactions from a natural bond orbital, donor-acceptor viewpoint. *Chem. Rev.* **1988**, *88*, 899-926.
- (42) Olsen, E. P. K.; Arrechea, P. L.; Buchwald, S. L. Mechanistic insight leads to a ligand which facilitates the palladium-catalyzed formation of 2-(hetero)arylaminooxazoles and 4-(hetero)arylaminothiazoles. *Angew. Chem. Int. Ed.* **2017**, *56*, 10569-10572.
- (43) McCann, S. D.; Reichert, E. C.; Arrechea, P. L.; Buchwald, S. L. Development of an aryl amination catalyst with broad scope guided by consideration of catalyst stability. *J. Am. Chem. Soc.* **2020**, *142*, 15027-15037.
- (44) Tkachov, R.; Senkovskyy, V.; Komber, H.; Sommer, J.-U.; Kiriy, A. Random catalyst walking along polymerized poly(3-hexylthiophene) chains in Kumada catalyst-transfer polycondensation. *J. Am. Chem. Soc.* **2010**, *132*, 7803-7810.
- (45) Jarrett-Wilkins, C. N.; Pollit, A. A.; Seferos, D. S. Polymerization catalysts take a walk on the wild side. *Trends Chem.* **2020**, *2*, 493-505.
- (46) Bautista, M. V.; Varni, A. J.; Ayuso-Carrillo, J.; Carson, M. C.; Noonan, K. J. T. Pairing Suzuki-Miyaura cross-coupling and catalyst transfer polymerization. *Polym. Chem.* **2021**, *12*, 1404-1414.